Published in final edited form as:
J Magn Reson. 2014 May ; 0: 18–22. doi:10.1016/j.jmr.2014.01.014.

^{19}F Spin-lattice Relaxation of Perfluoropolyethers: Dependence on Temperature and Magnetic Field Strength (7.0-14.1T)

Deepak K. Kadayakkara[1,2,5], **Krishnan Damodaran**[6], **T. Kevin Hitchens**[7], **Jeff W.M. Bulte**[1,2,3,4,5,*], and **Eric T. Ahrens**[8]

[1]Russell H. Morgan Dept. of Radiology and Radiological Science, Division of MR Research, The Johns Hopkins University School of Medicine, Baltimore, MD 21205

[2]Dept. of Oncology, The Johns Hopkins University School of Medicine, Baltimore, MD 21205

[3]Dept. of Biomedical Engineering, The Johns Hopkins University School of Medicine, Baltimore, MD 21205

[4]Dept. of Chemical & Biomolecular Engineering, The Johns Hopkins University School of Medicine, Baltimore, MD 21205

[5]Cellular Imaging Section, Institute for Cell Engineering, The Johns Hopkins University School of Medicine, Baltimore, MD 21205

[6]Department of Chemistry, University of Pittsburgh, Pittsburgh, PA

[7]Department of Biological Sciences, Carnegie Mellon University, Pittsburgh, PA; Pittsburgh NMR Center for Biomedical Research, Carnegie Mellon University, Pittsburgh, PA 15213

[8]Department of Radiology, University of California at San Diego, La Jolla, CA 92093

Abstract

Fluorine (^{19}F) MRI of perfluorocarbon labeled cells has become a powerful technique to track the migration and accumulation of cells in living organisms. It is common to label cells for ^{19}F MRI with nanoemulsions of perfluoropolyethers that contain a large number of chemically equivalent fluorine atoms. Understanding the mechanisms of ^{19}F nuclear relaxation, and in particular the spin-lattice relaxation of these molecules, is critical to improving experimental sensitivity. To date, the temperature and magnetic field strength dependence of spin-lattice relaxation rate constant (R_1) for perfluoropolyethers has not been described in detail. In this study, we evaluated R_1 of linear perfluoropolyether (PFPE) and cyclic perfluoro-15-crown-5 ether (PCE) at three magnetic field strengths (7.0, 9.4, and 14.1 T) and at temperatures ranging from 256-323K. Our results show that R_1 of perfluoropolyethers is dominated by dipole-dipole interactions and chemical shift anisotropy. R_1 increased with magnetic field strength for both PCE and PFPE. In

*Address Correspondence to: Jeff W.M. Bulte, Johns Hopkins University School of Medicine, Russell H. Morgan Department of Radiology and Radiological Science, Division of MR Research, 217 Traylor Bldg, 720 Rutland Ave, Baltimore, MD 21205, Phone 443-287-0996 Fax 443-287-7945, jwmbulte@mri.jhu.edu.

the temperature range studied, PCE was in the fast motion regime ($\omega\tau_c < 1$) at all field strengths, but for PFPE, R_1 passed through a maximum, from which the rotational correlation time was estimated. The importance of these measurements for the rational design of new ^{19}F MRI agents and methods is discussed.

1. Introduction

Cyclic perfluoro-15-crown-5 ether (PCE) and linear perfluoropolyether (PFPE) molecules with repeating -CF_2CF_2O- units are increasingly being used for cellular and molecular MRI [1-4]. The use of ^{19}F MRI has the advantage that there is no background signal in tissue, thus the imaging probe has high specificity. Moreover, quantification of the number of targeted probe molecules is feasible *in vivo* [5-6] leading to new cell tracking methods, such as *in vivo* cytometry [6]. For cell labeling, these molecules are formulated as an oil-in-water emulsion to enable use in biological applications [7]. PCE has desirable properties for imaging because each molecule has 20 chemically equivalent fluorine atoms giving rise to a single resonance peak. With these molecules, on the order of $10^{12} – 10^{13}$ fluorine atoms can be loaded into a cell of interest, providing a detection limit of order $10^4 – 10^5$ labeled cells per voxel [8]. One advantage of ^{19}F MRI cell tracking is that, with a known labeling efficiency, the cell number can be estimated from ^{19}F spin-density weighted images [5], for which the acquisition time is limited by R_1. Interestingly, unlike ^1H MRI of tissue water [9], spin-lattice relaxation rate constant (R_1) of PCE increases with increasing magnetic field strength [10], thereby allowing accelerated data acquisition at higher field strengths. PFPE is essentially a linear version of the cyclic PCE, which has a significantly long R_1 compared with PCE, making it an attractive label for *in vivo* cell tracking by MRI where enhanced imaging speed and sensitivity is desirable.

Understanding the molecular mechanisms of spin-lattice-relaxation in these two closely related molecules could aid the development of novel agents that are optimized for ^{19}F cellular MRI [7]. In this study, we measured the temperature dependence of ^{19}F R_1 for the linear PFPE and cyclic PCE between 256 K to 323 K at three different magnetic field strengths: 7.0 T (282 MHz), 9.4 T (376 MHz), and 14.1 T (564 MHz). These measurements were used to provide insight into the mechanisms ^{19}F nuclear spin-lattice relaxation in these molecules and to estimate the apparent rotational correlation times.

2. Experimental

Sample preparation

PCE and PFPE with 98% purity were obtained from Exfluor LP (Round Rock, TX) and used without further modification. The molecular weights of PCE and PFPE were 580 and 1000 Da, respectively. The viscosity of PCE was 4.8 Pa s and PFPE was 14.74 Pa s. 200 μl of neat PCE and PFPE oil were transferred to a 2.5 mm NMR tube and purged with 100% nitrogen for 15 minutes to remove oxygen. Tubes were sealed gas-tight with epoxy resin. PCE and PFPE emulsions were obtained from Celsense (Pittsburgh, PA) at a concentration of 120 mg/ml. Emulsion samples for NMR measurements were prepared in the same way as described above.

NMR measurements

^{19}F NMR measurements were made at 282, 376, and 564 MHz at temperatures between 256 to 323K using three different Bruker Avance III NMR spectrometers (Bruker Biospin, Billerica, MA). A 5mm Bruker QNP probe was used at 282 MHz and a BBFO-Plus probe was used at 376 and 564 MHz. On both these probes the inner radio frequency coil was used for ^{19}F observation. The probe temperature was calibrated using ethylene glycol by measuring the chemical shift difference between the OH and CH_2 resonance [11] before every measurement. The longitudinal relaxation time constant, T_1 ($1/R_1$) measurements were made using an inversion recovery sequence with phase cycling for a total of 8 averages per sample. A non-selective 90° pulse length of 15.5 μs was used and the recycle delay was 20s. 14 recovery points were used for each relaxation measurement. T_1 was determined with a two-parameter monoexponential fit using Topspin software (Bruker). The ^{19}F COSY spectrum was measured using 2048 and 128 TD points in the direct and indirect dimensions respectively with a recycle delay of 4 s and 8 scans were average per TD point in the F1 dimension. The data were processed with SI of 2048 × 1024. Spectral width of 100 ppm was used for both inversion recovery and COSY experiments. Data analysis was performed using Origin software (Originlab, Northampton, MA). The R_1 versus temperature data for PFPE was fit to a third degree polynomial. To calculate the maximum point, the first derivative of the fit was solved for $f'(T)=0$.

3. Results

The structures of PCE and PFPE are shown in Figures 1A and 1C, respectively. PCE has 20 fluorine atoms with equivalent chemical shifts at −92.8 ppm (Figure 1B) (relative to $CFCl_3$ (trichloro-fluoro-methane) at 0.00 ppm). PFPE is provided as a mixture of polymers with 28-36 fluorine atoms per molecule and major resonance peaks between −90.7 and −90.9 ppm that arise from the perfluoropolyether chain and minor peaks at −58 and −93 ppm that arises from the terminal perfluorocarbon moieties (Figure 1D). Theoretically, the fluorine atoms of perfluoropolyether backbone should only exhibit a single resonance peak; however, the large size and conformation of the molecule within the local environment can give rise to different chemical shifts. The range of chemical shifts could also result from a difference in the polymer chain lengths present in PFPE. The separation between two major resonance peaks (90.7 and 90.9 ppm) increases linearly with magnetic field ranging from 14 Hz (0.49 ppm) at 282 MHz, 19 Hz (0.50 ppm) at 376 MHz and 29 Hz (0.51 ppm) at 564 MHz, consistent with chemical shift separation and not spin-spin coupling, as this would display field independence. ^{19}F-COSY experiments further confirmed that there is no spin-spin coupling between these two major resonance peaks (Figure 1E). A broad-band COSY experiment showed that there is a weak correlation between the major peaks and minor peak supporting the assignment of the minor peak to the end groups (Figure 1F). T_1 was measured at three different magnetic field strengths (7.0, 9.4, and 14.1T) and at temperatures ranging from 256 K to 323 K. T_1 was estimated using a two-parameter monoexponential recovery curve (Figure 2A and C). For PCE, R_1 decreased with increasing temperature for this range for all magnetic field strengths (Figure 2B). For PFPE, R_1 was calculated using the area integrated over the two major resonance peaks. For all magnetic field strengths, R_1 increased with temperature from 256 K to reach a maximum before decreasing (Figure 2D).

To estimate the maximum point, the data was fit to a third order polynomial, followed by solving $f'(T) = 0$. The maximum R1 was observed at 281.6 K for 14.1T, 270.6 K for 9.4T and 264 K at 7T. No maximum was observed for PCE at these temperatures and magnetic field strengths. The T_1 of PCE and PFPE was then measured at 14.1 T in aqueous nanoemulsions for the same temperature range. The temperature dependence of R_1 was similar to that found for the neat preparations. For PCE, the R_1 decreased with increasing temperatures (Figure 3A), and R1 values of the nanoemulsions and neat preparations were similar. For PFPE, R_1 increased from 256 K to reach a maximum at 279.4 K and then decreased (Figure 3B). This temperature at which $f'(T) = 0$ is in good agreement with the neat measurement; however, for PFPE, the R_1 values were reduced by about 20% in the nanoemulsion.

We calculated the rotational correlation time (τ_c) for PFPE directly from the apparent maximum of R_1 versus temperature (Figure 2D). Assuming $\omega^2 \tau_c^2 = 1$ at the R_1 maximum, the calculated rotational correlation times for the neat PFPE were 1.77×10^{-9} s at 281.6 K, 2.66×10^{-9} s at 270.6 K, and 3.55×10^{-9} s at 264 K. For the PFPE emulsion, a rotational correlation time of 1.77×10^{-9} s was calculated at 279.4 K. As expected, an inverse linear relationship between rotational correlation time and temperature was observed. The rotational correlation time for PCE could not be calculated from the range of temperatures and magnetic field studied. Measurements at higher magnetic fields and/or lower temperatures would be needed to find the maximum for R_1.

4. Discussion and Conclusions

The temperature and field strength dependence of R_1 for perfluoropolyethers is consistent with contributions from dipole-dipole and CSA interactions [12-13].

$$R_1 = R_1^{dipole} + R_1^{CSA}$$

$$R_1^{dipole} = R_1^{rot} + R_1^{trans}$$

$$R_1^{rot} = \frac{1}{5} I(I+1)\gamma^4\hbar^2 r^{-6}\left[J(\omega) + 4J(2\omega)\right] \quad \text{Eq: 105, pg. 300, ref. 13}$$

$$R_1^{trans} = \frac{6\pi^2}{5}\gamma^4\hbar^2\frac{N\eta}{kT} \quad \text{Eq: 115, pg. 302, ref. 13}$$

$$R_1^{CSA} = \frac{6}{40}\gamma^2 B_0^2\delta^2\left(1+\frac{\eta^2}{3}\right)\left[J(\omega)\right] \quad \text{Eq: 141, pg. 316, ref.13}$$

where J(ω) is the spectral density function given by

$$J(\omega) = \frac{2\tau_c}{1+\frac{\omega^2}{\tau_c^2}}$$ Eq: 91, pg.297, ref.13

τ_c is the rotational correlation time and R_1 is a maximum at $\tau_c = 1/\omega$

Our measurements show that R_1 increases with increasing magnetic field strengths due to CSA. The contribution of CSA increases with increasing magnetic field with a dependence of B_0^2. For tissue water in the fast motion regime ($\omega\tau_c < 1$), dipole-dipole interactions dominate nuclear relaxation and R_1 decreases with increasing magnetic field strength. The observed trend of R_1 versus temperature for the perfluorocarbon molecules supports contributions from both dipole-dipole and CSA interactions. However, we did not attempt to quantify the relative contributions of these two relaxation mechanisms. We calculated the τ_c for PFPE using the assumption that $\omega^2 \tau_c^2 = 1$ at R1 maximum. From the equation for $R1^{rot}$, it follows that at R1 maximum, $4\omega^2 \tau_c^2 = 1$ can also be assumed. The range of temperatures did not allow us to separate the contributions of $J(\omega)$ or $J(2\omega)$, but exploring a larger temperature range may allow separation of the rotation ($J(\omega) + 4J(2\omega)$) from CSA contributions ($J(\omega)$). The decrease in R_1 from 293 K to 323 K for PFPE and 256 K to 323 K for PCE suggest that, at these temperatures, the molecules experience fast to intermediate tumbling motion within the NMR time scale ($\omega\tau_c < 1$). R_1 versus temperature trends observed in neat liquids at 14.1T were similar to that of the respective emulsions. For PFPE, the temperature at which the R_1 maximum was observed in emulsion was in good agreement with the R_1 maximum observed in neat liquid. However, unlike PCE, the PFPE R_1 was found to be about 20% lower in the emulsion compared to the neat liquid. The presence of residual O_2 in the neat liquid could contribute to relaxation, although all the samples were prepared by bubbling N_2 thought the samples. One could speculate that translational diffusion could be limited in the emulsion and translational intermolecular dipolar relaxation could make a significant contribution in the neat liquid.

In addition to temperature and magnetic field strengths, the spin-lattice relaxation of perfluorocarbons including perfluoropolyethers are influenced by the oxygen content. The paramagnetic properties of molecular oxygen increase the R_1 which has been used to measure tissue oxygenation *in vivo* [14, 15]. *In vitro* calibration studies at different magnetic field strengths have shown that R_1 exhibits a linear increase with pO_2 [10, 14, 15].

CSA is a predominant mechanism for NMR relaxation in many solids, however, in liquids, CSA components average out due to rapid tumbling motion. The motions that produce this average value can cause fluctuations in the local magnetic field, and these time-varying fields lead to relaxation [16]. Although PCE and PFPE are liquids in the temperature range studied, our data show that CSA makes a significant contribution to R_1. Perfluorocarbons are particularly interesting because of their low intermolecular dipole-dipole interactions and high vapor pressures compared to corresponding hydrocarbons of equal chain length. Low inter-molecular interactions are due to the large electronegativity of the F in C-F bonds, which effectively repel any other similar molecules in their vicinity [17].

Understanding the molecular dynamics underlying NMR relaxation, such as rotational correlation times can aid in the development of optimized perfluoropolyethers for ^{19}F MRI. The rotational correlation time for PFPE was calculated from the maximum R_1 versus temperature, but the rotational correlation time of PCE could not be determined since the molecule remained in the fast motion regime over the temperature and field strength used in our study. However, our relaxation data support a shorter effective rotational correlation time for PCE than PFPE at a given temperature, likely a result of the lower molecular weight and viscosity [18]. In addition, the shape of the molecules may also influence the rotational tumbling motion [19]. PFPE has a long chain, and the strong electronegativity of C-F bonds tends to align the chains in a rigid linear structure compared to PCE, where the crown-ether structure gives rise to a compact alignment.

The increase in R_1 with increasing magnetic field strength observed in perfluoropolyethers is desirable for imaging at high magnetic field strengths because signal-to-noise ratio per unit time can be increased with an optimized T1-weighted sequence. However, at high field strengths, increased CSA and magnetic field inhomogenieties can lead to undesirable line-broadening. For cell tracking, however, ^{19}F MRI is typically acquired at 2-4 times lower resolution than ^{1}H MRI, therefore, the effect of line broadening on signal localization can be minimal. PFPE has a long spin-spin relaxation time constant (T_2), which is also attractive for imaging applications. There are other perfluorocarbon molecules used for cellular imaging such as perfluorooctyl bromide [1, 2]; however, these molecules have multiple major resonance peaks over a broad chemical shift range resulting in a reduction in the sensitivity and confounding MRI results. Therefore, these molecules were not included in the study.

An ideal ^{19}F contrast agent for molecular MRI should have long R_1 and short R_2. Based on our measurements, for PFPE and PCE, R_1 can be increased by increasing magnetic field strengths. For PFPE, R_1 maximum was observed in the R1 versus temperature plots, from which we estimated the rotational correlation times. For *in vivo* imaging, it is desirable to have a R_1 maximum at about 310 K (37°C). From our data, a right shift in R_1 versus temperature plots could achieve it. A right shift in R_1 maximum towards 310 K was observed with increasing magnetic field strengths suggesting that PFPE is an optimized agent for high field MRI. For imaging at clinical field strengths of 3T and below, PFPE can be optimized by increasing the chain length. For PCE, enlarging the crown structure could result in more signals per molecule and more desirable R_1 characteristics. The emulsion formulation can be optimized by increasing the size of the emulsion droplets and viscosity of the emulsions into an acceptable range without affecting the stability of the emulsion. For ex vivo imaging of tissues, the sensitivity can be increased by reducing the temperature of the samples. Understanding the fundamental principles of ^{19}F NMR relaxation of these molecules will aid in the rational design of ^{19}F contrast agents.

Acknowledgments

We are grateful to Dr. Paul A. Bottomley for his helpful discussion and insight into relaxation mechanisms. This work was supported in part by the National Institutes of Health (R01 CA134633, R01 EB17271 and P41 EB 001977), the Maryland Stem Cell Research Foundation (MSCRFII-0161), and the California Institute for Regenerative Medicine (LA1-C12-06919).

References

[1]. Chen J, Lanza GM, Wickline SA. Quantitative magnetic resonance fluorine imaging: today and tomorrow. WIRES Nanomed. Nanobi. 2010; 2:431–440.

[2]. Ruiz-Cabello J, Barnett BP, Bottomley PA, Bulte JWM. Fluorine (19F) MRS and MRI in biomedicine. NMR Biomed. 2011; 24:114–129. [PubMed: 20842758]

[3]. Ahrens ET, Flores R, Xu H, Morel PA. In vivo imaging platform for tracking immunotherapeutic cells. Nature Biotechnol. 2005; 23:983–987. [PubMed: 16041364]

[4]. Bulte JW. Hot spot MRI emerges from the background. Nature Biotechnol. 2005; 23:945–946. [PubMed: 16082363]

[5]. Srinivas M, Morel PA, Ernst LA, Laidlaw DH, Ahrens ET. Fluorine-19 MRI for visualization and quantification of cell migration in a diabetes model. Magn. Reson. Med. 2007; 58:725–734. [PubMed: 17899609]

[6]. Srinivas M, Turner MS, Janjic JM, Morel PA, Laidlaw DH, Ahrens ET. In vivo cytometry of antigen-specific t cells using 19F MRI. Magn. Reson. Med. 2009; 62:747–753. [PubMed: 19585593]

[7]. Janjic JM, Ahrens ET. Fluorine-containing nanoemulsions for MRI cell tracking. WIREs Nanomed. Nanobi. 2009; 1:492–501.

[8]. Ahrens ET, Zhong J. In vivo MRI cell tracking using perfluorocarbon probes and fluorine-19 detection. NMR Biomed. 2013; 26:860–71. [PubMed: 23606473]

[9]. Bottomley PA, Foster TH, Argersinger RE, Pfeifer LM. A review of normal tissue hydrogen NMR relaxation times and relaxation mechanisms from 1-100 MHz: dependence on tissue type, NMR frequency, temperature, species, excision, and age, Medical physics. 1984; 11:425–448.

[10]. Duong TQ, Iadecola C, Kim SG. Effect of hyperoxia, hypercapnia, and hypoxia on cerebral interstitial oxygen tension and cerebral blood flow, Magnetic resonance in medicine : official journal of the Society of Magnetic Resonance in Medicine/Society of Magnetic Resonance in Medicine. 2001; 45:61–70.

[11]. Raiford DS, Fisk CL, Becker ED. Calibration of methanol and ethylene glycol nuclear magnetic resonance thermometers. Anal. Chem. 1979; 51:2050–2051.

[12]. Bloembergen N, Purcell EM, Pound RV. Relaxation Effects in Nuclear Magnetic Resonance Absorption. Phys. Rev. 1948; 73:679–712.

[13]. Abragam, A. The principles of nuclear magnetism. Clarendon Press; Oxford: 1961.

[14]. Dardzinski BJ, Sotak CH. Rapid tissue oxygen tension mapping using 19F inversion-recovery echo-planar imaging of perfluoro-15-crown-5-ether, Magnetic resonance in medicine : official journal of the Society of Magnetic Resonance in Medicine/Society of Magnetic Resonance in Medicine. 1994; 32:88–97.

[15]. Kadayakkara DK, Janjic JM, Pusateri LK, Young WB, Ahrens ET. In vivo observation of intracellular oximetry in perfluorocarbon-labeled glioma cells and chemotherapeutic response in the CNS using fluorine-19 MRI, Magnetic resonance in medicine : official journal of the Society of Magnetic Resonance in Medicine/Society of Magnetic Resonance in Medicine. 2010; 64:1252–1259.

[16]. Gerig, J. Fluorine NMR. Monograph published online. 2001. p. 1-35.Available from http://www.biophysics.org/portals/1/pdfs/education/gerig.pdf

[17]. Neilson, AH. Organofluorines. Springer; Berlin: 2002. Partitioning of Organofluorine Compounds in the Environment; p. 68-69.

[18]. Debye, PJW. Polar molecules. The Chemical Catalog Company, inc; New York: 1929.

[19]. Hu CM, Zwanzig R. Rotational Frictional Coefficients for Spheroids with Slipping Boundary-Condition. J. Chem. Phys. 1974; 60:4354–4357.

Highlights

1. T1 of perfluoropolyethers can be explained by dipole-dipole interactions and CSA
2. Molecular motion determines the differences in R_1 between PCE and PFPE
3. The rotational correlation time of PFPE was estimated from R_1 vs. temp plots

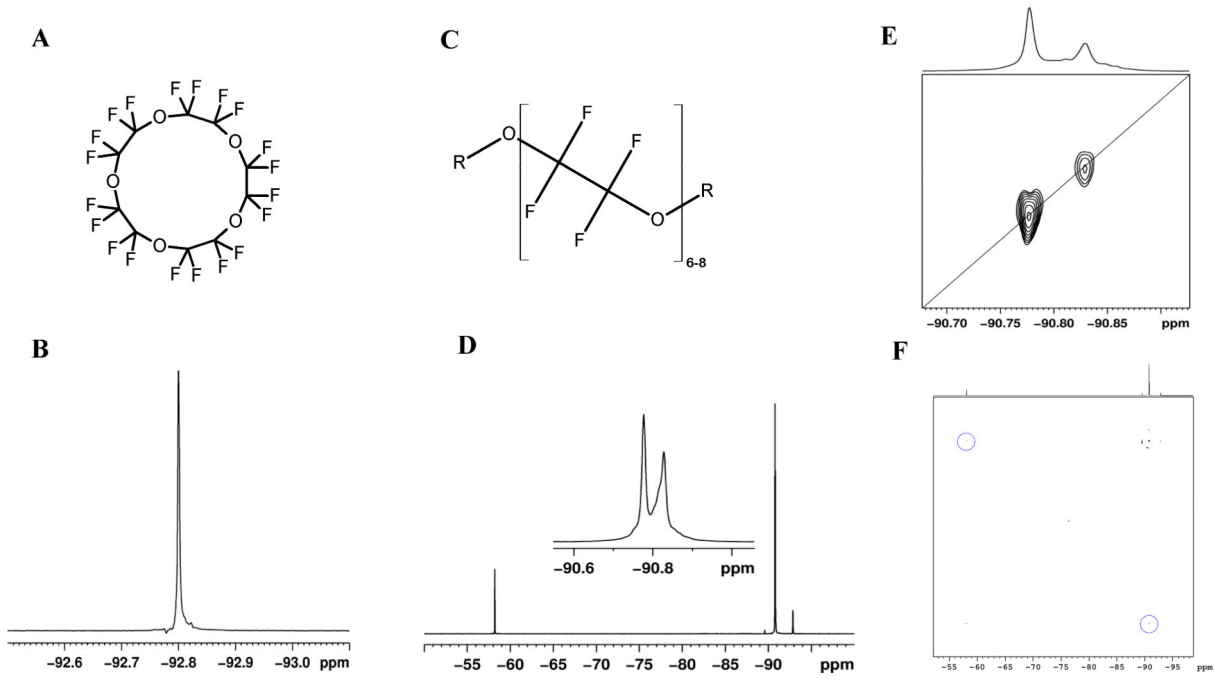

Figure 1.

Structure and ^{19}F NMR spectra of PCE and PFPE. (A) Structure of PCE and (C) PFPE (R=CF_2CF_3 or CF_3). (B) PCE has 20 equivalent ^{19}F atoms showing a single peak at −92.8 ppm. (D) PFPE has about 28-36 ^{19}F atoms with two major chemical shifts at −90.7 and −90.9 ppm. The inset shows the magnified view of the major peaks. (E) ^{19}F COSY shows that there is no spin-spin coupling between the peaks. (F) ^{19}F COSY spectrum of PFPE at broad bandwidth shows a weak correlation between major and minor resonances supporting the assignment of minor peak to the endgroup of the molecule

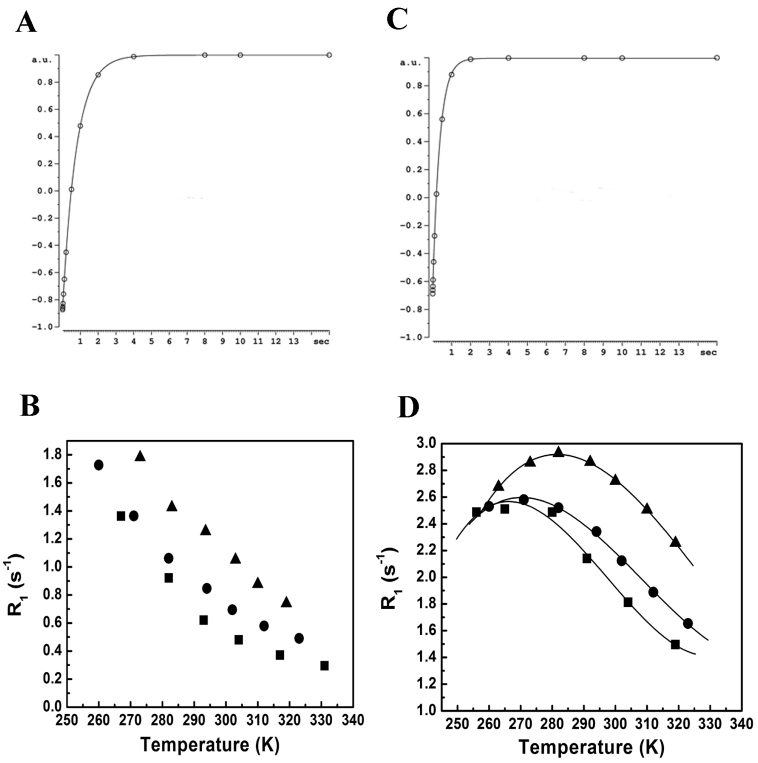

Figure 2.

R_1 versus temperature at 7.0, 9.4, and 14.1T. (A) A representative mono-exponential R_1 inversion recovery curve of PCE and (C) PFPE. (B) R_1 decreased with temperature and increased with magnetic field strength for PCE. (D) For PFPE, R_1 increased from 256 K until a maximum and then decreased. The data were fit to a third degree polynomial, and the maximum point was determined by solving $f'(T)=0$. The R_1 maximum was observed at 281.63 K (14.1T), 270.61 K (9.4T), and 264 K (7.0T). The rotational correlation time for PFPE was estimated to be 1.77×10^{-9} s at 281.63 K, 2.66×10^{-9} s at 270.61 K, and 3.55×10^{-9} s at 264 K. At all temperatures and magnetic field strengths, PCE has a slower R_1 compared to PFPE. (▲) = 14.1 T, (●) = 9.4 T, and (■) = 7.0 T.

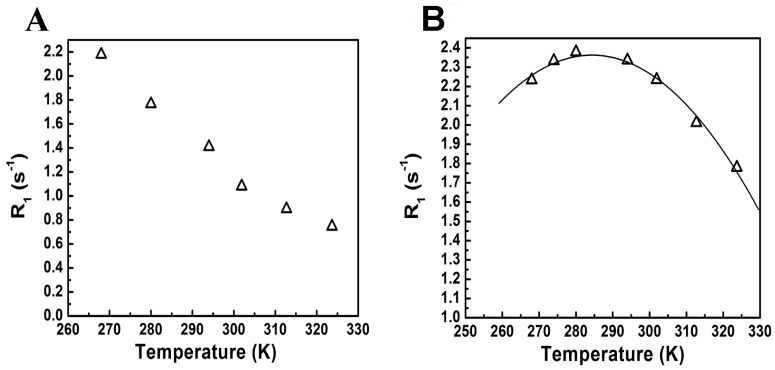

Figure 3.

R_1 versus temperature of PCE and PFPE emulsions at 14.1T. (A) R_1 decreased with temperature for PCE emulsions. B) For PFPE, R_1 increased from 268 K until a maximum and then reduced. The data were fit to a third degree polynomial, and the maximum point was determined by solving $f'(T)=0$. The R1 maximum was observed at 279. 4 K.